Electronic Supplementary Material (ESI) for Nanoscale.

Supporting information for: Morphology of gold nanoparticles determined by full-curve fitting of the absorption spectrum. Comparison with X-ray scattering and electron microscopy data

Kostyantyn Slyusarenko,* Benjamin Abécassis, Patrick Davidson, and Doru Constantin*

Laboratoire de Physique des Solides, Univ. Paris-Sud, CNRS, UMR8502, 91405 Orsay Cedex, France.

E-mail: kslyusarenko@gmail.com; doru.constantin@u-psud.fr

*To whom correspondence should be addressed

TEM data

Particle analysis

In Figure S1, we show the aspect ratio X as a function of the radius R for all the particles used in the analysis (each panel displays the objects from two synthesis batches).

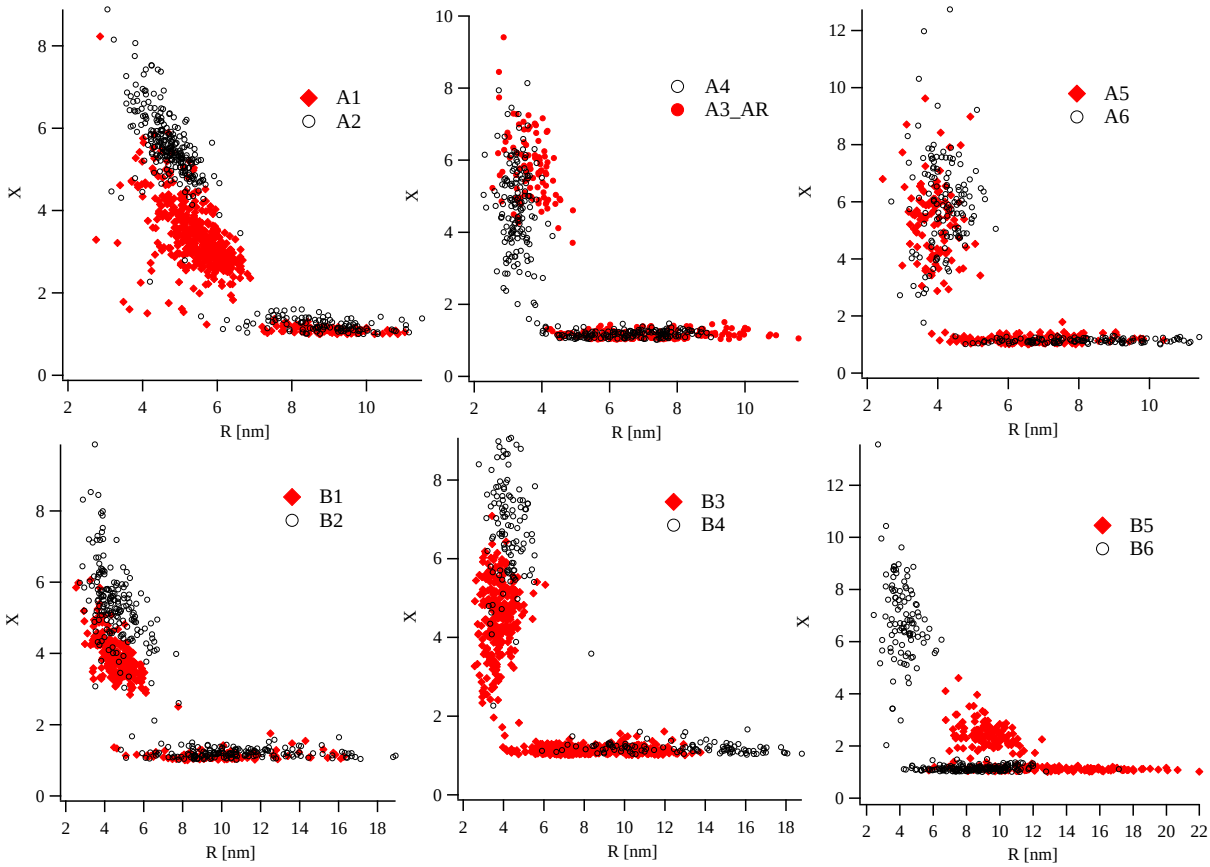

Figure S1: Aspect ratio as a function of the radius for all the objects (both rods and spheres).

Particle volume and correlation with the aspect ratio

The theoretical model assumes that the volume V and the aspect ratio X of the rods are uncorrelated. In Figure S2 we plot $V = \pi R_R^2 L$ versus $X = L/(2R_R)$ for all the rods (symbols) and the best linear fit to $V(X)$. The slope $\mathrm{d}V/\mathrm{d}X$ is given in Figure S3. Although this parameter is significantly different from zero for most samples, its value is randomly

distributed over the entire series. Setting it to zero (i.e. neglecting the correlation between V and X) is thus a reasonable pragmatic decision when aiming for a general model.

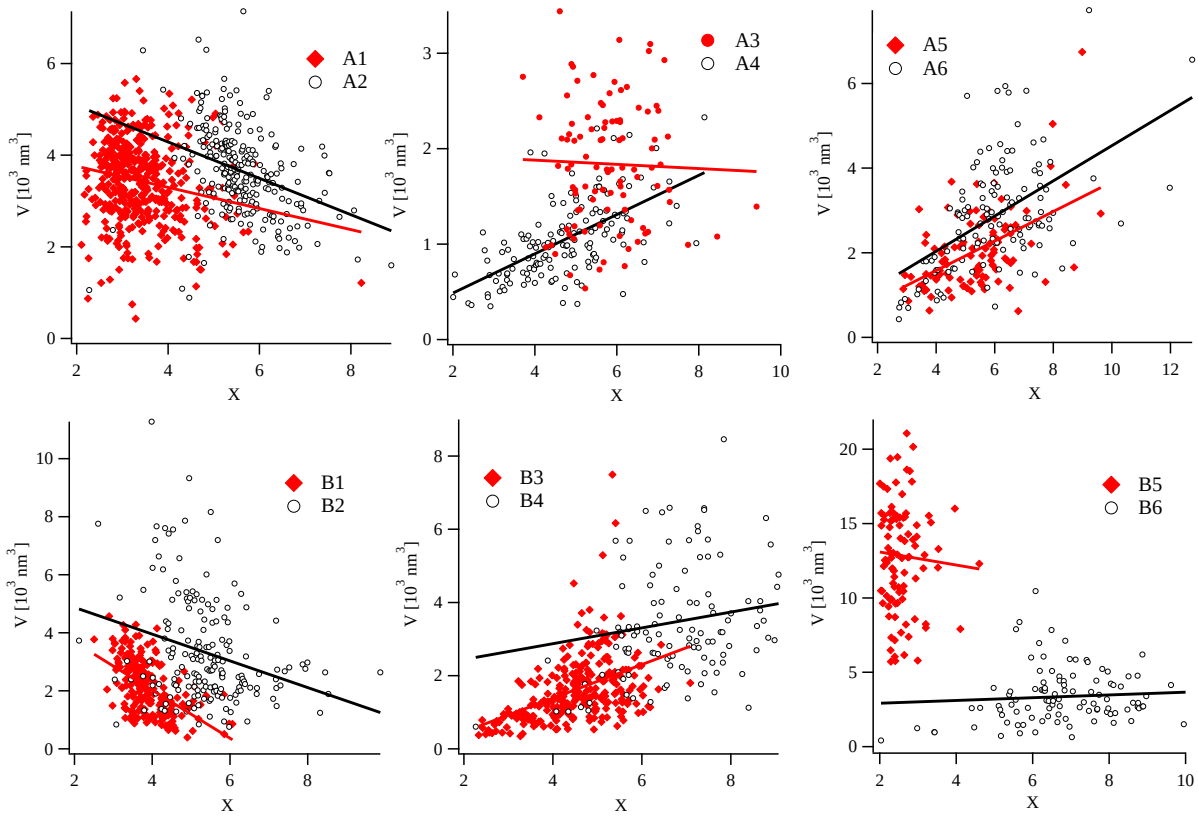

Figure S2: Estimated volume $V = \pi R_R^2 L$ as a function of the aspect ratio $X = L/(2R_R)$ for all the rods (various symbols) and linear fits to $V(X)$. The fit slopes are shown in Figure S3.

AS model: simplified relations

From extensive simulations of the theoretical model (Equation (1) in the main text) we extracted simplified relations between the relevant parameters:

- the absorption spectrum is characterized by the position $\lambda_{\max}$ and amplitude H_{lp} of the longitudinal peak as well as its full width at half maximum W, and by the amplitude of the transverse peak H_{tp}.

- the nanoparticle suspensions are characterized by the aspect ratio of the nanorods

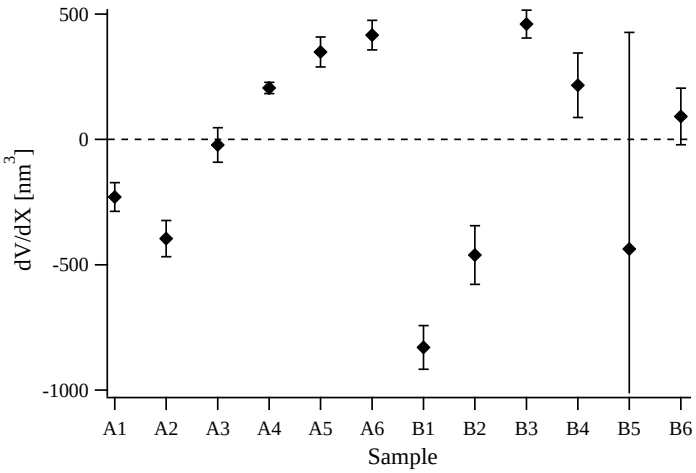

Figure S3: Slope dV/dX of the linear fits in Figure S2. The error bars indicate the fit uncertainty (one standard deviation).

X and its relative dispersion $\varepsilon_X = \sigma_X/X$, as well as the concentration of rods and spheres, ϕ_R and ϕ_S. The results also depend weakly on R_R/A and R_S/A, where R_R and R_S are the radii of the rods and spheres and A is the damping parameter defined in Equation (2) of the main text.

Each simulated spectrum was fitted with the following function:

$$A_{\lambda,fit}(\lambda) = B_1 \exp(-a_1\lambda) + B_2 \exp(-a_2\lambda) + \frac{A_1}{\sigma_1\lambda\sqrt{2\pi}} \exp\frac{(\ln\lambda - \mu_1)^2}{2\sigma_1^2} + \frac{A_2}{\sigma_2\lambda\sqrt{2\pi}} \exp\frac{(\ln\lambda - \mu_2)^2}{2\sigma_2^2}, \tag{1}$$

where the wavelength λ is expressed in nm and B_1, a_1, B_2, a_2, A_1, μ_1, σ_1, A_2, μ_2, σ_2 are adjustable parameters. The first and the third terms describe the peak at 518 nm (sum of the plasmonic resonance in the spheres and the transverse resonance in the rods) and the second and the fourth terms describe the longitudinal resonance in the rods. Parameters $\lambda_{\max}$ and W are obtained as:

$$\lambda_{\max} = \exp(\mu_2 - \sigma_2^2) \tag{2a}$$

$$W^2 = 8\log 2 \exp(2\mu_2 + \sigma_2^2)[\exp(\sigma_2^2) - 1] \tag{2b}$$

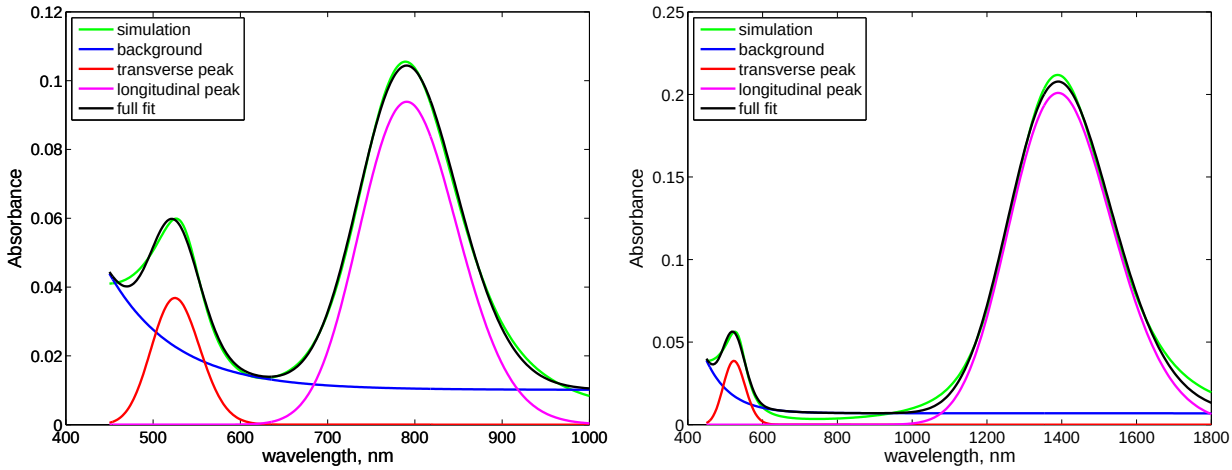

Figure S4: Absorption spectrum simulated using Equation (1) in the main text and fit with the function $\gamma_{\text{fit}}(\lambda)$ (1) for two aspect ratios: $X = 4$ (left) and $X = 10$ (right). The other parameters are identical for the two simulations: $\varepsilon_X = 0.1$, $\phi_R = \phi_S = 4.4 \cdot 10^{-7}$, $R_R/A = 14.3\,\text{nm}$ and $R_S/A = 100\,\text{nm}$. The three terms in the fit function are also shown.

The dependence of $\lambda_{\max}$ and W (both in nm units) on X and ε_X for a fixed value $R_R/A = 14.3\,\text{nm}$ is shown in Figure S5. The polynomial interpolation is given by (3). The converse dependence (of X and ε_X on $\lambda_{\max}$ and W) is more useful in practice. It is presented in Figure S6 (also included in the main text as Figure 7) and the corresponding interpolation is given in (4).

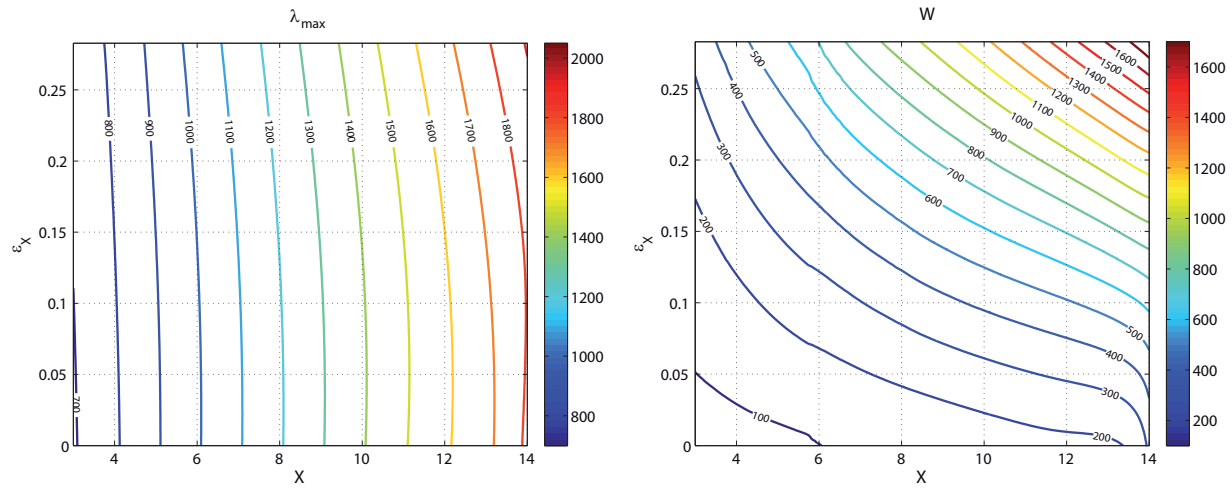

Figure S5: Position $\lambda_{\max}$ (left) and width W (right) of the longitudinal peak of the nanorods simulated by Equation (1) in the main text as a function of X and ε_X (for $R_R/A = 14.3\,\text{nm}$) represented as color-coded level curves.

$$\lambda_{\max}(X, \varepsilon_X) = 394.4 + 98.69X + 0.07853X^2 + 134.4\varepsilon_X - 394.7\varepsilon_X^2 - 24.28\varepsilon_X X + 171\varepsilon_X^2 X \tag{3a}$$

$$\begin{aligned} W(X, \varepsilon_X) = {} & 29.5 + 9.269X + 0.2907X^2 + 307.9\varepsilon_X - 1407\varepsilon_X^2 + 148.9\varepsilon_X X \\ & + 725.7\varepsilon_X^2 X + 2.618\varepsilon_X X^2 \end{aligned} \tag{3b}$$

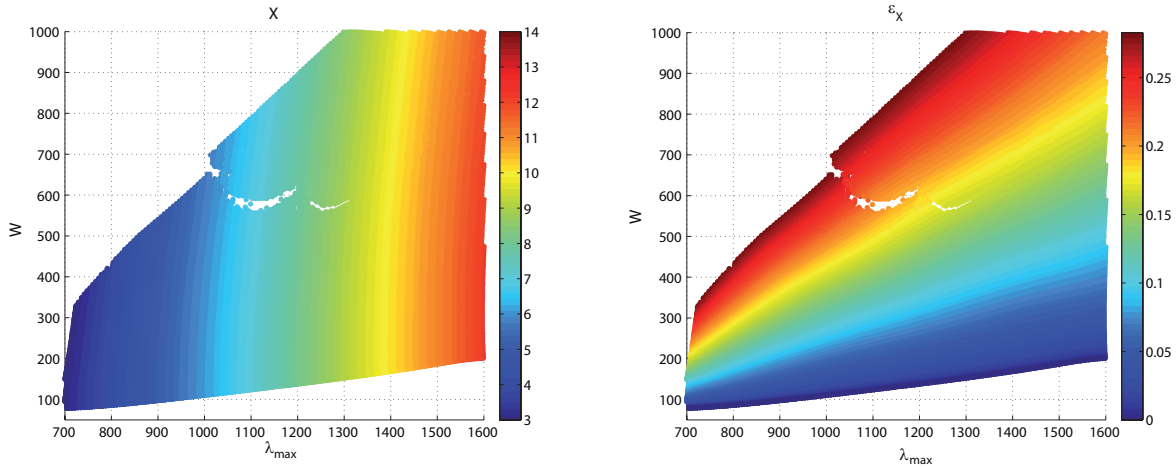

Figure S6: Aspect ratio X (left) and relative variance ε_X (right) of the nanorod population simulated by Equation (1) in the main text as a function of $\lambda_{\max}$ and W (for $R_R/A = 14.3\,\mathrm{nm}$) represented as color code. Reproduces Figure 7 in the main text.

$$\begin{aligned} X(\lambda_{\max}, W) = {} & -8.155 + 0.060\lambda_{\max} - 0.6061W - 0.000109\lambda_{\max}^2 + 0.0013\lambda_{\max}W \\ & - 0.00056W^2 + 5.08 \cdot 10^{-8}\lambda_{\max}^3 - 5.69 \cdot 10^{-7}\lambda_{\max}^2 W \\ & + 3.74 \cdot 10^{-7}\lambda_{\max}W^2 - 1.93 \cdot 10^{-8}W^3 \end{aligned} \tag{4a}$$

$$\begin{aligned} \varepsilon_X(\lambda_{\max}, W) = {} & 1.408 - 0.2256\lambda_{\max} + 0.9768W + 0.00041\lambda_{\max}^2 - 0.00197\lambda_{\max}W \\ & + 0.000704W^2 - 1.73 \cdot 10^{-7}\lambda_{\max}^3 + 8.89 \cdot 10^{-7}\lambda_{\max}^2 W \\ & - 5.43 \cdot 10^{-7}\lambda_{\max}W^2 + 7.097 \cdot 10^{-8}W^3 \end{aligned} \tag{4b}$$

For a given morphology, the height of the longitudinal peak H_{lp} is proportional to the volume concentration of the nanorods ϕ_R. We can write the latter as:

$$\phi_R = 10^{-7} \frac{H_{\mathrm{lp}}}{H^{\star}_{\mathrm{lp}}}, \tag{5}$$

where $H^{\star}_{\mathrm{lp}}$ is the amplitude of the longitudinal peak simulated by the model for $\phi_R = 10^{-7}$ (with $R_R/A = 14.3$ nm), see Figure S7 and is interpolated by the polynomials (6). We emphasize that both H_{lp} and $H^{\star}_{\mathrm{lp}}$ are *amplitudes*, i.e. the heights of the peaks with respect to their backgrounds, and not the raw peak values. The distinction is particularly relevant for small aspect ratio, see e.g. Figure S4.

$$\begin{aligned} H^{\star}_{\mathrm{lp}}(X, \varepsilon_X) = {} & -0.03127 + 0.05944X - 0.05944\varepsilon_X - 0.002907X^2 - 0.241X\varepsilon_X \\ & + 5.427\varepsilon_X^2 + 7.765 \cdot 10^{-5}X^3 + 0.003201X^2\varepsilon_X + 0.3961X\varepsilon_X^2 - 12.18\varepsilon_X^3 \end{aligned} \tag{6a}$$

$$\begin{aligned} H^{\star}_{\mathrm{lp}}(\lambda_{\max}, W) = {} & 0.1748 + -0.001527\lambda_{\max} + 0.001773W + 3.541 \cdot 10^{-6}\lambda_{\max}^2 \\ & - 6.213 \cdot 10^{-6}\lambda_{\max}W + 1.943 \cdot 10^{-6}W^2 - 2.376 \cdot 10^{-9}\lambda_{\max}^3 + 3.627 \cdot 10^{-9}\lambda_{\max}^2 W \\ & + 1.712 \cdot 10^{-9}\lambda_{\max}W^2 - 2.815 \cdot 10^{-9}W^3 + 5.515 \cdot 10^{-13}\lambda_{\max}^4 - 7.542 \cdot 10^{-13}\lambda_{\max}^3 W \\ & - 7.711 \cdot 10^{-13}\lambda_{\max}^2 W^2 + 7.116 \cdot 10^{-13}\lambda_{\max}W^3 + 3.672 \cdot 10^{-13}W^4 \end{aligned} \tag{6b}$$

The volume concentration of the spheres is:

$$\phi_S = 3.28 \cdot 10^{-6} \left[H_{\mathrm{tp}} - H^{\star}_{\mathrm{tp}}\, 10^7 \cdot \phi_R \right] = 3.28 \cdot 10^{-6} \left[H_{\mathrm{tp}} - H^{\star}_{\mathrm{tp}} \frac{H_{\mathrm{lp}}}{H^{\star}_{\mathrm{lp}}} \right], \tag{7}$$

where ϕ_R is given by (5) and with:

$$H^{\star}_{\mathrm{tp}} = 0.012 + 0.0035 \cdot X^{-1} + 0.05 \cdot X^{-2} \tag{8}$$

and H_{tp} is the absorbance at the position of the transverse peak (518 nm).

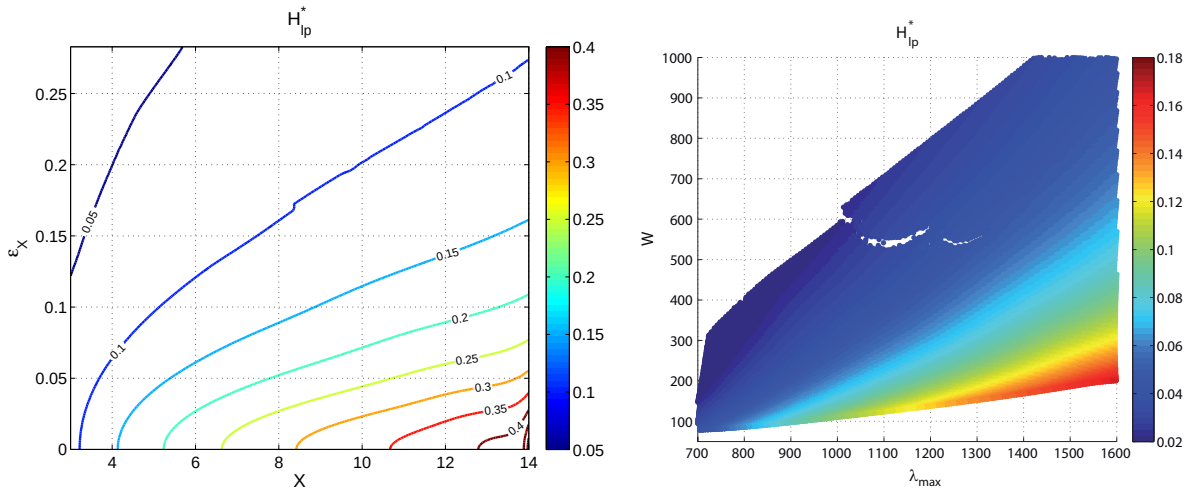

Figure S7: Amplitude $H^\star_{\rm lp}$ of the longitudinal peak for $\phi_R = 10^{-7}$. Left: as a function of (X, ε_X), from Equation (6a) (color-coded level curves). Right: as a function of $(\lambda_{\rm max}, W)$, from Equation (6b) (color code).

So far, we have set $R_R/A = 14.3\,$nm, a value close to the experimental results. Furthermore, $\lambda_{\rm max}$ and W only weakly depend on this parameter. For completeness, we give below formulas for this dependence:

$$\lambda_{\rm max} = \lambda_{\rm max}^{14.3}(1.003 - 0.045\, A/R_R) \tag{9a}$$

$$W = W^{14.3}(0.880 + 1.694\, A/R_R) \tag{9b}$$

where $\lambda_{\rm max}^{14.3}$ and $W^{14.3}$ are the values for $R_R/A = 14.3\,$nm obtained in Equations (3).

Alternative estimate for the concentration

Spheres The literature value for the atomic extinction coefficient of spherical gold nanoparticles (at the wavelength of the plasmon peak) is $\epsilon_{\mathrm{S}} = 3900 - 4000\,\mathrm{M}^{-1}\mathrm{cm}^{-1}$.[S1,S2] The corresponding absorbance is $A_{\mathrm{S}} = l c_{\mathrm{Au}} \epsilon_{\mathrm{S}}$, where c_{Au} is the molarity of gold atoms and l the optical path through the sample (1 cm in our experiments). The volume concentration of spheres then reads:

$$\phi_S = \frac{c_{\mathrm{Au}} M_{\mathrm{Au}}}{10^3 \rho_{\mathrm{Au}}} = \frac{A_{\mathrm{S}} M_{\mathrm{Au}}}{10^3 l \epsilon_{\mathrm{S}} \rho_{\mathrm{Au}}}, \tag{10}$$

where $M_{\mathrm{Au}} = 197\,\mathrm{g}$ is the molar mass and $\rho_{\mathrm{Au}} = 19.3\,\mathrm{g/cm}^3$ is the density of gold.

Rods In the case of nanorods, the absorbance depends on the molar extinction coefficient of the particles as $A_{\mathrm{R}} = l c_{\mathrm{Au}} \epsilon_{\mathrm{R}}$ and the formula for the volume fraction is in all points similar to (10), except for the absorbance being evaluated at the position of the longitudinal plasmon resonance:

$$\phi_R = \frac{c_{\mathrm{Au}} M_{\mathrm{Au}}}{10^3 \rho_{\mathrm{Au}}} = \frac{A_{\mathrm{R}} M_{\mathrm{Au}}}{10^3 l \epsilon_{\mathrm{R}} \rho_{\mathrm{Au}}}, \tag{11}$$

Here, however, the extinction coefficient ϵ_{R} depends on the aspect ratio of the particles. Fitting the literature data[S3] to a straight line yields the approximation:

$$\epsilon_{\mathrm{R}} = (7263\,X - 6224)\,\mathrm{M}^{-1}\mathrm{cm}^{-1} \tag{12}$$

By extrapolating this dependence to the aspect ratio of our nanorods (taken from the TEM data) we obtain ϕ_R. The sum of ϕ_S and ϕ_R, normalized by the value ϕ_{SAXS} obtained from the SAXS data is plotted as open dots in Figure 2 of the main text.

The dielectric constant of bulk gold

In describing the absorbance of the nanoparticles, the dielectric constant of bulk gold $\epsilon_{\mathrm{bulk}}(\lambda) = \epsilon_1(\lambda) + i\epsilon_2(\lambda)$ is a fundamental ingredient. Several sets of data were published,[S4–S8] showing

significant differences, in particular in the imaginary component ϵ_2, which is strongly affected by the presence of defects (Figure S8).

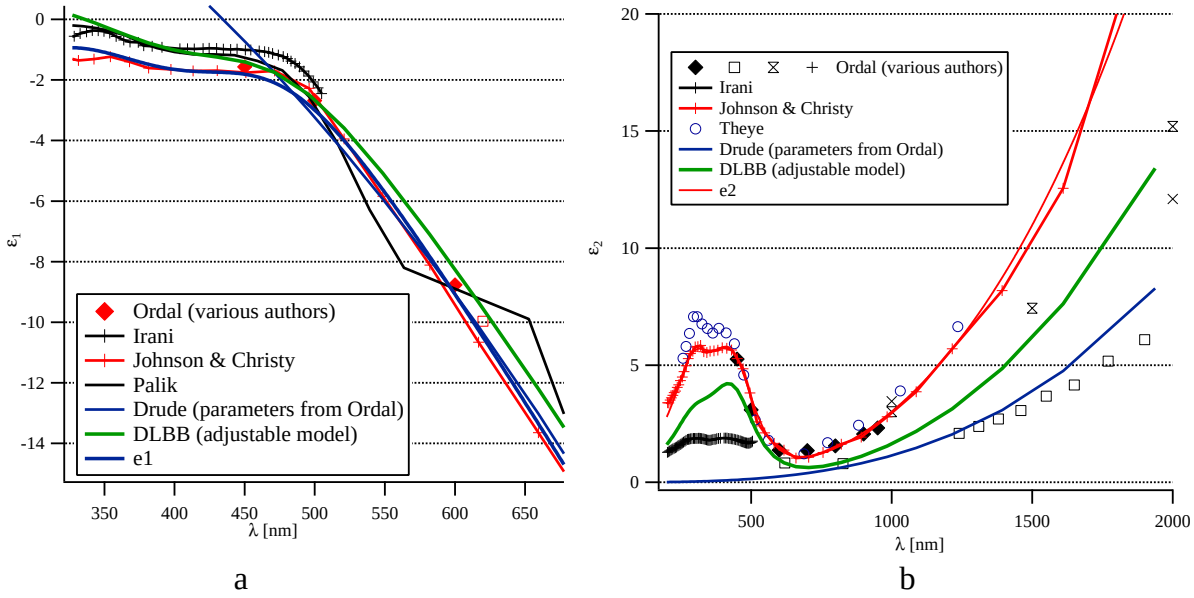

Figure S8: Wavelength dependence of the complex dielectric constant of gold, as given by several authors (lines and symbols): a – real part $\epsilon_1(\lambda)$; b – imaginary part $\epsilon_2(\lambda)$. The values used in this work are shown as solid green line and correspond to model (13) with parameters given in Table S1

.

A very convenient analytical model, combining the Drude-Lorentz contribution and two interband transitions (DLBB) was proposed by Etchegoin et al.[S9],[S10]. For instance, with appropriate values for the parameters, the model describes very well the data of Johnson and Christy[S5]. We therefore use it in the following. The model is given in Equation (13) and the parameters in Table S1.

$$\epsilon_{\text{bulk}}(\lambda) = \epsilon_\infty - \frac{1}{\lambda_p^2[1/\lambda^2 + i/(\gamma_p\lambda)]} + \sum_{1,2} \frac{A_i}{\lambda_i}\left[\frac{\exp(i\varphi_i)}{(1/\lambda_i - 1/\lambda - i/\gamma_i)} + \frac{\exp(-i\varphi_i)}{(1/\lambda_i + 1/\lambda + i/\gamma_i)}\right] \tag{13}$$

We chose the parameter values such that $\epsilon_2(\lambda)$ is roughly in the middle of the experimental points from various authors (Figure S8b) and $\epsilon_1(\lambda)$ agrees with the experimental data below

Table S1: Parameter values for the analytical DLBB model (13), for the data of Johnson and Christy[S5] (from S9 and S10) and those used in this paper. The λ and γ are given in nanometres, while φ_1 and φ_2 are in radians. Values modified in our treatment with respect to S5 are given in bold.

Parameter	ϵ_∞	λ_p	γ_p	A_1	φ_1	λ_1	γ_1	A_2	φ_2	λ_2	γ_2
Johnson and Christy[S5]	1.54	143	14500	1.27	$-\pi/4$	470	1900	1.1	$-\pi/4$	325	1060
This work	**4**	**146**	**25000**	**1**	$-\pi/4$	470	1900	**0.5**	$-\pi/4$	325	1060

500 nm (Figure S8a). Above this value, the behaviour of $\epsilon_1(\lambda)$ is mainly determined by λ_p, which we fix at 146 nm, rather than the 143 nm given by Johnson and Christy[S5], by calibrating our model against recent data[S11] for the dependence of $\lambda_{\max}$ on the aspect ratio X of gold nanorods (see Figure S9).

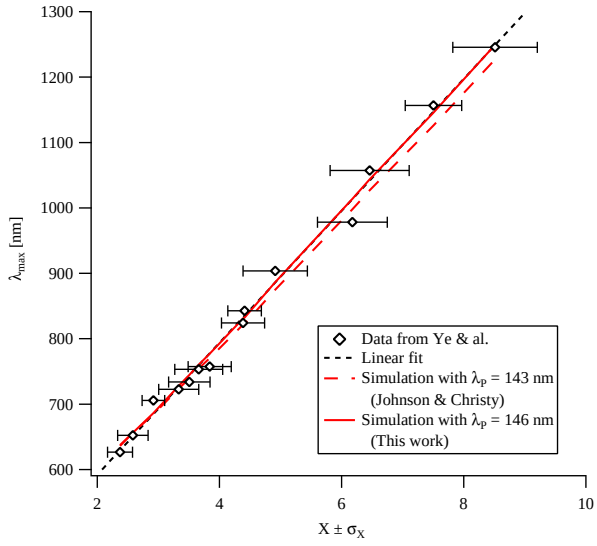

Figure S9: Experimental data for the dependence of $\lambda_{\max}$ on X, from Ye *et al.*,[S11] Figure S27b ($\diamond$). The error bars represent the variance σ_X. Linear fit (dotted line) and prediction of our model (Equation 1 in the main text) with $R_R/A = 14.3\,\mathrm{nm}$, for $\lambda_p = 146\,\mathrm{nm}$ (solid line) and for $\lambda_p = 143\,\mathrm{nm}$ (dashed line).

References

(S1) Link, S.; Wang, Z. L.; El-Sayed, M. A. Alloy Formation of Gold-Silver Nanoparticles and the Dependence of the Plasmon Absorption on Their Composition. *The Journal of Physical Chemistry B* **1999**, *103*, 3529–3533.

(S2) Mulvaney, P.; Giersig, M.; Henglein, A. Surface chemistry of colloidal gold: deposition of lead and accompanying optical effects. *The Journal of Physical Chemistry* **1992**, *96*, 10419–10424.

(S3) Orendorff, C. J.; Murphy, C. J. Quantitation of metal content in the silver-assisted growth of gold nanorods. *The Journal of Physical Chemistry B* **2006**, *110*, 3990–3994.

(S4) Irani, G.; Huen, T.; Wooten, F. Optical constants of silver and gold in the visible and vacuum ultraviolet. *JOSA* **1971**, *61*, 128–129.

(S5) Johnson, P. B.; Christy, R. W. Optical constants of the noble metals. *Phys. Rev. B* **1972**, *6*, 4370.

(S6) Palik, E. D. *Handbook of Optical Constants of Solids*; Academic Press, 1991.

(S7) Ordal, M. A.; Long, L. L.; Bell, R. J.; Bell, S. E.; Bell, R. R.; Alexander, R. W., Jr.; Ward, C. A. Optical properties of the metals Al, Co, Cu, Au, Fe, Pb, Ni, Pd, Pt, Ag, Ti, and W in the infrared and far infrared. *Applied Optics* **1983**, *22*, 1099.

(S8) Thèye, M.-L. Investigation of the Optical Properties of Au by Means of Thin Semi-transparent Films. *Physical Review B* **1970**, *2*, 3060–3078.

(S9) Etchegoin, P. G.; Le Ru, E. C.; Meyer, M. An analytic model for the optical properties of gold. *The Journal of Chemical Physics* **2006**, *125*, 164705.

(S10) Etchegoin, P. G.; Le Ru, E. C.; Meyer, M. Erratum: "An analytic model for the optical properties of gold" [J. Chem. Phys.125, 164705 (2006)]. *The Journal of Chemical Physics* **2007**, *127*, 189901.

(S11) Ye, X.; Jin, L.; Caglayan, H.; Chen, J.; Xing, G.; Zheng, C.; Doan-Nguyen, V.; Kang, Y.; Engheta, N.; Kagan, C. R.; Murray, C. B. Improved Size-Tunable Synthesis of Monodisperse Gold Nanorods through the Use of Aromatic Additives. *ACS Nano* **2012**, *6*, 2804–2817.